Mine Water and the Environment (2020) 39:797–807
https://doi.org/10.1007/s10230-020-00721-7

TECHNICAL ARTICLE

Comparison of APTES-Functionalized Silica Fiber and Clinoptilolite for Reducing Iron Concentrations in an Acidic Iron(II) Sulfate Solution: Potential Passive Treatment Substrates

Wes R. Sandlin[1] · Jeff B. Langman[1] · Kristopher V. Waynant[2] · Mausumi Mukhopadhyay[3] · Thomas Thuneman[4] · James G. Moberly[4]

Received: 29 February 2020 / Accepted: 17 September 2020 / Published online: 3 October 2020

Abstract

Passive treatment systems provide lower cost alternatives for remediation of mine drainage; however, acidic drainage increases treatment difficulty because of higher metal concentrations and proton competition for reactive substrates. A silica fiber functionalized with (3-aminopropyl) triethoxysilane (Si + APTES) and a naturally-occurring, microporous silicate mineral (clinoptilolite of the zeolite family) were evaluated in the laboratory as potential reactive substrates for passive treatment of mild (≥ pH of 3) acid rock drainage. Column permeability experiments with spun, 10-µm median diameter, silica fiber and loosely packed, 3.6-mm median diameter clinoptilolite indicate greater permeability and stability of clinoptilolite under flowing conditions. Batch sorption experiments with silica fiber (Si), Si + APTES, and clinoptilolite in a synthetic Fe(II)–SO_4, pH 3.0 solution indicate an Fe specific sorption efficacy of Si + APTES > clinoptilolite > Si at equivalent surface areas. Specific sorption normalized to packing densities indicate greater sorption per volume for clinoptilolite. Sorption results for Si + APTES and clinoptilolite did not produce isotherms described by the Langmuir or Freundlich models, likely because of surface heterogeneity and precipitation reactions. Column sorption experiments under flowing conditions indicate an Fe removal efficacy of clinoptilolite > Si + APTES for permeable packing densities. Si + APTES demonstrated high specific sorption of Fe in batch sorption experiments and has potential use in low-flow, passive treatment of mildly acidic solutions. The balance of minimal surface preparation, greater permeability, structural stability, large surface area, micropore structure, and ion-exchange properties make clinoptilolite a better reactive substrate for passive treatment of mildly acidic solutions in high- or low-flow conditions.

Keywords Iron sorption · Reactive substrate · Acid rock drainage · Zeolite · Aminosilane

Introduction

The generation of acid rock drainage (ARD) from the weathering of sulfidic ore and waste rock continues to significantly degrade local and regional water resources (Fig. 1) across the United States and around the globe (Akcil and Koldas 2006; Benner et al. 1999; Nordstrom 2009). In particular, abandoned mines are difficult sites for reduction or treatment of mine drainage (Johnson and Hallberg 2005). In an attempt to treat mine drainage and other sources of poor-quality drainage, passive treatment systems were developed to reduce contaminant concentrations, minimize health risks, and lower treatment costs (Johnson and Hallberg 2005). Such systems have shown mixed results treating ARD because of proton [H^+] competition and seasonality of discharge and metal concentrations (Costello 2003; Fryar

✉ Jeff B. Langman
jlangman@uidaho.edu

1 Department of Geological Sciences, University of Idaho, Moscow, ID, USA

2 Department of Chemistry, University of Idaho, Moscow, ID, USA

3 Department of Chemical Engineering, National Institute of Technology, Surat, Gujarat, India

4 Department of Chemical and Biological Engineering, University of Idaho, Moscow, ID, USA

and Schwartz 1998; Sandlin et al. 2020), which indicate the need for additional passive treatment systems and associated reactive substrates for ARD remediation.

The quality of mine drainage typically is proportional to the acidity of the drainage (Kefeni et al. 2017; Nordstrom and Alpers 1999), which is driven by the oxidation of iron-sulfide minerals and subsequent release and mobility of iron [Fe] and other metals (Bigham and Nordstrom 2000; Dold 2017; Egiebor and Oni 2007; Nordstrom 2011; Nordstrom et al. 2015). Passive treatment of poor-quality mine drainage includes biological, geochemical, and physical processes to improve water quality through reduction of acidity and metal concentrations (Skousen et al. 2017). Inorganic (e.g. calcite) or organic (e.g. mulch) substrates for use in treatment systems induce metal capture through sorption and/or changes in acidity and/or reduction–oxidation potential that induce mineral precipitation (Gibert et al. 2004; Skousen et al. 2017). Metal capture on inorganic substrates can be viewed as the combination of ligand availability and sorption and/or precipitation to hydrous oxide surfaces (Davis and Leckie 1978; Dzombak and Morel 1990; Stumm and Morgan 1996). Sorption typically occurs through electrostatic interaction between metals in solution and a negatively charged surface (commonly the oxide of another metal), which can be influenced by surface site availability, sorption of metals at neighboring sites, and cation competition (Stumm and Morgan 1996).

Metal capture by sorption on silicate substrates, such as zeolites and clays, is common for treatment of wastewater (Faghihian et al. 1999; Pandová et al. 2018; Yavuz et al. 2003), but silicate substrates typically are not used for ARD treatment because of their limited point of zero charge (pH_{pzc}). The presence of competing protons in ARD influences metal sorption (Dzombak and Morel 1990; Heidmann et al. 2005) through neutralization of the residual negative surface charge (surface protonation) of reactive materials (Nelson et al. 2019). Artificial and natural silicate substrates, such as silica glass and zeolite minerals, tend to have a pH_{pzc} near 3 (Cotton 2008; Gainer 1993), which makes such substrates applicable for treating weakly (> 4.5) to mildly (> 3.0) acidic solutions.

Fig. 1 Example of acid rock drainage impacting a creek in the Great Falls coal field near Stockett, Montana

For this study, a manufactured silicate material (fused silica fiber) functionalized with (3-aminopropyl) triethoxysilane (Si + APTES) and a natural silicate substrate (clinoptilolite $[(Na,K,Ca)_{2-3}Al_3(Al,Si)_2Si_{13}O_{36}{\cdot}12H_2O]$) were evaluated at the benchtop scale for potential use as reactive substrates in a high-flow ARD passive treatment system. Bare silica (Si) fiber was included for comparison of a glass surface without the presence of a chelator. The goal of the study was to determine the potential applicability of these low cost, readily available, and easily prepared substrates for capturing Fe under mildly acidic conditions in an idealized acidic, Fe(II)-SO_4 solution. This idealized solution was synthetically produced in the lab for benchtop testing of the substrates to initially evaluate their metal capture (sorption + precipitation) capabilities, given proton competition within acidic conditions. This validation testing allowed for control of solution conditions and comparison of sorption capabilities of each substrate. Such testing is necessary for selecting appropriate reactive substrates for site-specific conditions and testing under more variable conditions.

Materials and Methods

The selected Si fiber (Technical Glass Products, Inc., Painesville, Ohio) is a non-crystalline quartz (fused glass) spun to a wool from fibers of 5–15 µm in diameter (Fig. 2). The specific surface area of the Si fiber (assumed 10-µm diameter) was calculated from a density of 0.016 g/cm^3, a specific volume of 0.45 cm^3/g, a total length (continuous height (h; Eq. 1) of the fiber in the specific volume equal to 5787 m/g, which produces a specific surface area (A) of 18 m^2/g (Eq. 2).

$$h = \frac{V}{\pi r^2} \tag{1}$$

$$A = 2\pi rh + 2\pi r^2 \tag{2}$$

The Si fiber was factory-coated on both sides with a starch binder (4–5% by weight) for ease of handling (Fig. 2). The weaving of the fiber into a wool provides torsion and bending resistance but still allows it to be manipulated (e.g. rolled, packed) for structural resistance to the flow of water.

Clinoptilolite (zeolite family [hydrated $(Na,K,Ca)_{2\text{-}6}Al_xSi_yO_z$]) are microporous, aluminosilicate grains derived from volcanic activity but also are synthetically produced (Burakov et al. 2018; Pandová et al. 2018). Zeolites can capture metals by sorption, as well as cation exchange, and are commonly referred to as "molecular sieves" because of their micropore structure (Holub et al. 2013; Motsi et al. 2009; Pandová et al. 2018; Stylianou et al. 2007; Wang and Peng 2010). For this study, clinoptilolite grains of 2.4–4.8 mm in diameter (4 × 8 mesh) were obtained from KMI Zeolite Inc., in Nevada (Fig. 3). Specific surface area of the clinoptilolite is estimated by the manufacturer to be 40 m^2/g. This type of zeolite typically has a 10- and 8-ring (framework element) micropore structure, which is considered a larger ring size in the zeolite family (Baerlocher et al. 2007). Prior to experimental use, clinoptilolite grains were triple-rinsed with reverse-osmosis filtered (ultrapure) water and dried at 80 °C to remove clinoptilolite dust generated during mining and handling.

Substrate Permeability

The permeability of bare Si fiber and 4 × 8 mesh clinoptilolite were examined in flow experiments using 5-cm diameter, PVC columns. These experiments were conducted by filling a 40-cm long column with either rolled Si fiber or loosely packed clinoptilolite. Bare Si fiber was tightly rolled and inserted into the column perpendicular to the rolling direction. This configuration allows structural resistance against collapse under flowing conditions. Si fiber packing densities of 0.073, 0.037, and 0.018 g/cm^3 were tested in this rolled configuration. Clinoptilolite was poured into the column, allowing the grains to freely settle, which produced a packing density of 0.73 g/cm^3. Hydrostatic pressure directed water from a 57-L container through the column and into a collection container (Fig. 4) where the effluent flow rate was measured. Flow rates were measured after 1 min to allow for full saturation and settling of each substrate. A constant head of 34 L (0.3 m depth) was maintained throughout the experiment with a peristaltic pump that recirculated water from the lower to upper container. Methylene blue was added as a tracer to the Si fiber permeability experiments for observing possible preferential flow or bypass with the various packing densities.

Surface Functionalization

The selected Si fiber represents a synthetic surface that can readily be functionalized with a chelator, such as silanization where ethoxy groups hydrolyze and form covalent Si–O–Si bonds with the silica surface (Liu et al. 2013). Branched polyethylenimine (PEI, $[H(NHCH_2CH_2)_nNH_2]$) and (3-aminopropyl) triethoxysilane (APTES, $[C_9H_{23}NO_3Si]$) were considered for potential use as chelators that could easily be applied to the Si fiber. Preliminary tests indicated greater ease of use (lower viscosity) and superior surface coverage with APTES, which was selected for surface functionalization of Si fiber for all sorption experiments. The clinoptilolite was not processed for chelator functionalization because of known issues with clogging/surface area reduction of the micropore structure with chelators such as APTES (Felice et al. 2013; Kassab et al. 2012; Wingenfelder et al. 2005), although application of APTES to clinoptilolite has shown improved performance for capture of CO_2 (Vilarrasa-García et al. 2015).

The amine functional groups of APTES are effective for metal chelation/capture in a variety of solutions (Barquist 2009; Ramasamy et al. 2017, 2018). APTES was applied to the Si fiber per methods developed by Acres et al. (2012) and Liu et al. (2013). The desired amount of Si fiber was

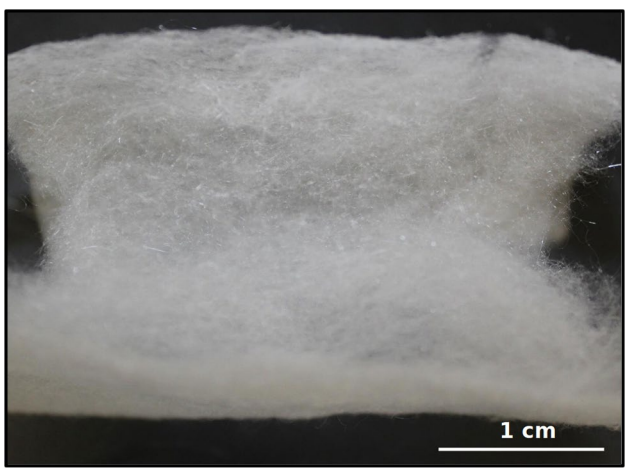

Fig. 2 Silica fiber spun into a wool with a starch coating

Fig. 3 Clinoptilolite grains, 2.4–4.8 mm diameter (4 × 8 mesh)

submerged in a 2% APTES (98% EtOH) solution for 20 min while agitated on an orbital shaker. Following submergence and agitation, Si + APTES was removed and repeatedly rinsed with 100% EtOH and ultrapure water. Rinsed Si + APTES were dried in an oven at 80 °C for 15 h. The Si fibers were not treated with an oxidizer, such as piranha solution (mixture of H_2SO_4 and H_2O_2), prior to functionalization (Acres et al. 2012; Zhu et al. 2012), because this would have removed the starch coating that is crucial to its structural integrity.

Preparation of Acidic Fe(II)–SO_4 Solution

Acidic Fe(II)–SO_4 solutions were prepared for the sorption experiments at Fe concentrations of 25–1000 mg/L by dissolving an appropriate mass of ferrous sulfate heptahydrate [$FeSO_4$•$7H_2O$] in ultrapure water. Sulfuric acid [H_2SO_4] was added to solutions until an initial pH of 3.0 was obtained and stable while solutions were mixed on an orbital shaker at 100 rpm for 30 min.

Batch Sorption Experiments

Batch sorption experiments were conducted with equivalent surface areas (216 m^2) of each substrate by inserting 12 g of Si, 12 g of Si + APTES, and 5.4 g of clinoptilolite in individual polyester mesh bags (three replicates) and suspending them in the acidic Fe(II)–SO_4 solutions [25, 50, 75, 100 mg/L] at 25 °C. A pH of 3.0 ± 0.1 was maintained throughout each experiment by introduction of concentrated H_2SO_4 (monitored by pH probe). The substrates were suspended in the acidic Fe(II)–SO_4 solutions in 1 L beakers and agitated on a shaker table for 4–6 h until sorption equilibrium occurred (stabilization of solution Fe concentration). Fe concentrations were measured with a Hach 3900 spectrophotometer and FerroVer reagent. Quality control and accuracy checks were performed over the course of the experiments with instrument blanks, replicate samples, and calibration standards. No false positive results were indicated, and replicate results were within acceptable range (± 10%) for Fe concentration. Specific sorption values (q; mg/g) were calculated for batch and column (small- and large-scale column experiments described below) sorption experiments:

$$q = \frac{C_i - C_f}{M} \tag{3}$$

where C_i and C_f are initial and final concentrations of Fe (mg/L), respectively, and M is substrate mass (mg/L).

Fig. 4 Laboratory setup for permeability column experiments

Adsorption Isotherms

Specific sorption values for each substrate were compared to Langmuir and Freundlich isotherm models to evaluate possible sorption characteristics. The Langmuir isotherm model assumes a homogeneous surface with a finite number of monolayer sorption sites (Langmuir 1918):

$$q_e = q_{max}\frac{K_L C_e}{1 + K_L C_e} \tag{4}$$

where q_e is the amount adsorbed (mg/g) at an equilibrium concentration (C_e, mg/L), q_{max} is the maximum monolayer adsorption (mg/g), and K_L is the Langmuir constant related to free energy of adsorption (Holub et al. 2013). The Freundlich isotherm model assumes a heterogeneous surface where adsorption can occur in multiple layers (Erdem et al. 2004; Holub et al. 2013; Limousin et al. 2007):

$$q_e = K_f C_e^{\frac{1}{n}} \tag{5}$$

where K_f is the Freundlich constant related to maximum adsorption capacity (mg/g) and n is a constant related to adsorption intensity (Fan and Zhang 2018; Holub et al. 2013).

Small-Scale Column Experiments

Small-scale column experiments were conducted by inserting 15 g of Si + APTES or 150 g of clinoptilolite (packing densities of 0.073 and 0.73 g/cm^3, respectively) into a PVC column of 5-cm diameter × 10-cm length (Fig. 5). The Si + APTES was tightly rolled into a cylindrical form prior to insertion into the column to provide sufficient structural integrity during wetting and to maximize surface area availability. A peristaltic pump directed the acidic Fe(II)–SO_4 solution (1000 mg/L) to the bottom of the flow column, through the permeable substrates, out the top of the column, and into a waste container at a rate of 25 mL/min and 12 mL/min for Si + APTES and clinoptilolite, respectively (slowest possible rates given resistance to flow). Effluent solution was collected at 0, 7.5, 15, 30, 60, 90, 120, 150, 180, 240, 300, and 360 min. The Fe concentration of the effluent was measured with a Hach DR3900 spectrophotometer until sorption site exhaustion of each substrate (effluent Fe concentration equal to influent concentration). Three replicate experiments were conducted in sequential order for each substrate. Following each experiment, the experimental apparatus was cleaned in a 15% HNO_3 solution and rinsed with ultrapure water.

In both the small- and large-scale (described below) column experiments, the mass of removed Fe was determined by subtracting effluent Fe concentration from influent Fe concentration. The area under the breakthrough curve attained by integrating the difference in concentration (C_{rem}; mg/L) vs time (min) was used to find the total Fe removed (R_{total}; mg) for a given pumping rate (Q) (Eq. 6; Aksu and Gönen 2004).

$$R_{total} = \frac{Q}{1000}\int_{t=0}^{t=t_{total}} C_{rem}dt \quad (6)$$

Large-Scale Column Experiments

Large-scale column experiments were conducted by inserting 600 g of clinoptilolite (0.73 g/cm^3 packing density) in a PVC column of 5-cm diameter × 40-cm length (Fig. 6). A peristaltic pump directed acidic Fe(II)–SO_4 solution (1000 mg/L) to the bottom of the flow column, through the clinoptilolite grains, out the top of the column, and into a waste container at a rate of 12 mL/min. Effluent solution was collected at 0, 0.5, 0.75, 1, 1.5, 2, 4, 6, 8, 14, 20, 26, 32, 38, 44, 50, 56, 62, 68, 74, 80, 86, 92, 98, and 104 h. Total Fe concentration was measured with a Hach DR3900 spectrophotometer until surface site sorption exhaustion (effluent concentration = influent concentration). Large-scale column experiments were conducted sequentially in triplicate.

Fig. 5 Example of small-scale column experiment

Clinoptilolite Surface Analysis

Pre- and post-experiment clinoptilolite surface morphology and Fe distribution were analyzed using a scanning electron microscope (Zeiss SUPRA 35 SEM) equipped with energy dispersive X-ray spectroscopy (Noran System Six EDS) at the University of Idaho Electron Microscopy Center. Samples were carbon-coated prior to analysis. Clinoptilolite surfaces were imaged for an evaluation of potential changes in

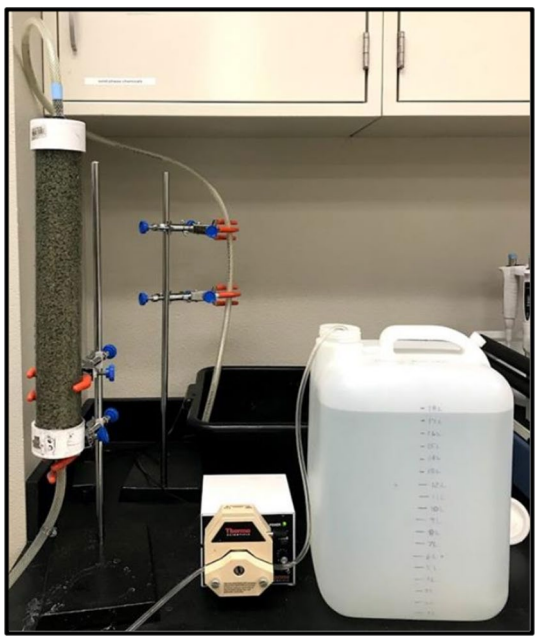

Fig. 6 Example of large-scale column experiment

surface morphology and distribution of captured Fe across the grain surface.

Results and Discussion

Substrate Permeability

Results of the permeability experiments indicate that clinoptilolite at a 4 × 8 mesh, grain-size distribution has greater permeability than all Si fiber packing densities. Measured flow rates through Si fiber at packing densities of 0.073, 0.037, and 0.018 g/cm^3 were 0.06, 0.08, and 0.14 L/s, respectively. Results indicate that the flow rate increased at lower packing densities; however, dye tracers revealed that preferential flow was occurring within the column at packing densities of 0.037 and 0.018 g/cm^3. At a packing density of 0.073 g/cm^3, Si fiber is a supported (no collapse of the structure with flow) and permeable packing arrangement that did not induce preferential flow. In all packing densities, Si fiber retained substantial water in void space that appeared to limit permeability. Clinoptilolite grains were slightly compacted after saturation and flow, but permeability remained at 0.20 L/s for the duration of the experiments. This flow rate is nearly three times the supported Si fiber flow rate of 0.073 g/cm^3. From the permeability results, packing densities of 0.073 g/cm^3 for Si fiber/Si + APTES and 0.73 g/cm^3 for clinoptilolite were selected for use in batch sorption calculations and column experiments.

Batch Sorption and Adsorption Isotherms

Specific sorption of Fe^{2+} by bare Si fiber was minimal for all Fe concentrations; therefore, further experimentation with bare Si fiber was abandoned. Sorption of Fe on Si + APTES and clinoptilolite increased as Fe concentration increased (Fig. 7). Specific sorption of Fe^{2+} at all concentrations was greater for Si + APTES compared to clinoptilolite (Fig. 7). However, specific sorption values are not indicative of how the substrates would perform in a passive treatment system because a greater mass (and surface area) of clinoptilolite can be packed into a similar volume. For this reason, specific sorption values were multiplied by packing densities of 0.073 and 0.73 g/cm^3 for Si + APTES and clinoptilolite, respectively (Fig. 8). Results indicate that a greater amount of Fe^{2+} was sorbed per volume (mg/cm^3) for clinoptilolite compared to Si + APTES (Fig. 8).

Neither the Langmuir or Freundlich isotherms were representative of the specific sorption results for Si + APTES and clinoptilolite. R^2 values calculated for the Langmuir isotherms were 0.545 and 0.544 for Si + APTES and clinoptilolite, respectively (Table 1). The chelating functional group of Si + APTES and the micropore structure

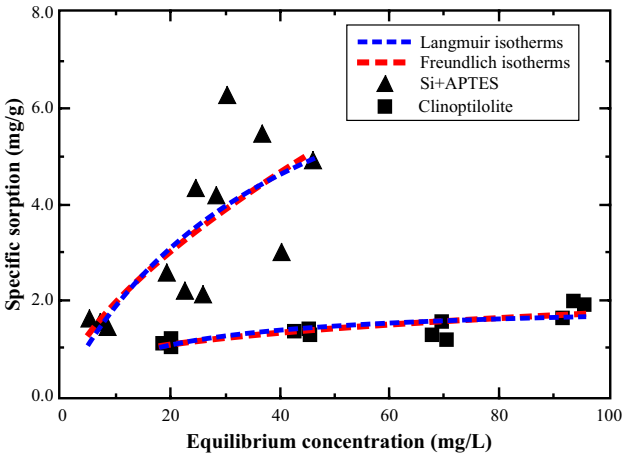

Fig. 7 Equivalent surface area adsorption equilibria of Fe^{2+} on Si + APTES and clinoptilolite at pH of 3.0 and Fe concentrations of 25, 50, 75, 100 mg/L with associated Langmuir and Freundlich isotherms

of clinoptilolite create heterogeneous surfaces, and it is unlikely that sorption occurred in a monolayer as predicted by the Langmuir model. R^2 values calculated for the Freundlich isotherms were 0.541 and 0.632 for Si + APTES and clinoptilolite, respectively (Table 1). The Freundlich model does not represent metal capture by Si + APTES because Fe removal is occurring by adsorption and chelation rather than just adsorption. The Freundlich model is a better fit for clinoptilolite because the model assumes a heterogeneous surface where multilayer sorption can occur, which is an applicable assumption for the variable topography of a clinoptilolite surface. Overall, neither model appropriately describes metal removal by Si + APTES or clinoptilolite surfaces, which may result from Fe precipitation processes in addition to sorption. All post-experiment Si + APTES and clinoptilolite surfaces changed color (Fig. 9), suggestive of Fe (oxyhydr)oxide precipitation as a result of capture and interaction with the substrate surfaces.

Sorption Under Flowing Conditions

Results from small-scale column experiments with 150 g of clinoptilolite (6000 m^2 surface area), 15 g of Si + APTES (270 m^2 surface area), and acidic, 1000 mg/L Fe(II)-SO_4 solution indicate greater Fe removal by clinoptilolite. Sorption site exhaustion occurred at ≈ 60 min for Si + APTES and 360 min for clinoptilolite (Fig. 10). Values for total Fe removal (R_{total}) were normalized by substrate mass and surface area, indicating equivalent Fe removal per g (R_M; mg/g) by both substrates, and a greater Fe removal per m^2 of surface area (R_{SA}) by Si + APTES (Table 2). For both substrates, Fe (oxyhydr)oxide precipitation occurred because of unidentified acid-neutralizing processes, resulting in rapid

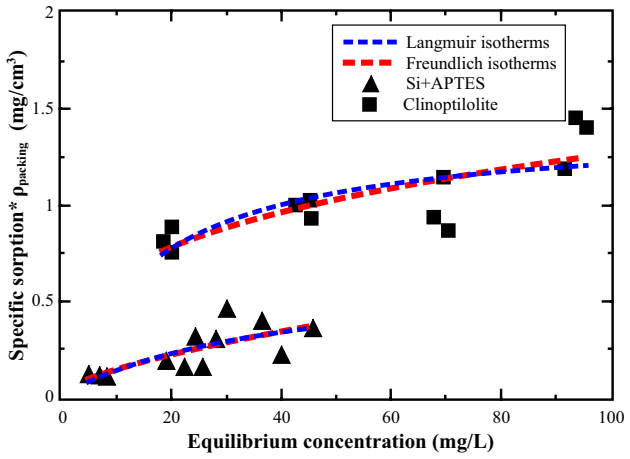

Fig. 8 Packing-density normalized adsorption equilibria of Fe^{2+} on Si + APTES and clinoptilolite at pH of 3.0 and Fe concentrations of 25, 50, 75, 100 mg/L with associated Langmuir and Freundlich isotherms

increases in effluent pH from 3.0 to 6.3 for Si + APTES and 3.0 to 5.9 for clinoptilolite (Fig. 11). As small-scale column experiments continued, effluent pH gradually decreased to 3.0 for Si + APTES and 3.4 for clinoptilolite (Fig. 11).

Given greater permeability, structural integrity, and normalized Fe removal for clinoptilolite, large-scale column experiments were used to evaluate potential changes in Fe removal with an increase in flow path length through the same loosely packed, clinoptilolite grain structure. Results indicate that quadrupling the amount of clinoptilolite from small to large column experiments increased time to sorption site exhaustion by a factor of 17 (Fig. 12). Normalized R_{total} values indicate that the longer flow path length of the large-scale column experiments increased Fe removal by nearly 50 mg/g and 1.5 mg/m^2 (Table 2).

Table 1 Parameter estimates for Langmuir and Freundlich isotherm models for experimental results of Fe^{2+} adsorption on Si + APTES and clinoptilolite at a solution pH of 3.0

Model type	Si + APTES	Clinoptilolite
Langmuir isotherm		
K_L^a (L/mg)	0.024 ± 0.028	0.061 ± 0.027
q_{max}^b (mg/g)	9.225 ± 6.164	1.936 ± 0.214
R^{2c}	0.545	0.544
Freundlich isotherm		
K_f^d (mg/g)	0.436 ± 0.356	0.436 ± 0.135
n^e	1.564 ± 0.590	3.337 ± 0.849
R^2	0.541	0.632

K_L^a Langmuir constant related to free energy of adsorption, q_{max}^b maximum monolayer adsorption, R^{2c} coefficient of determination, K_f^d Freundlich constant related to maximum adsorption, n^e constant related to sorption intensity

Initial column effluent increased in pH from 3.0 to 7.0, resulting in Fe (oxyhydr)oxide precipitation, followed by a gradual decrease of pH to 3.7 by the end of the experiments (Fig. 12).

Clinoptilolite Sorption Trends

In both small- and large-scale column sorption experiments, Fe removal was initially high and decreased exponentially, followed by a linear trend in surface passivation of the clinoptilolite with continual Fe removal (Figs. 10 and 12). The large removal of Fe from solution during the initial period of the small- and large-scale column experiments likely was due to the corresponding pH change, which decreased Fe solubility and resulted in precipitation of Fe (oxyhydr)oxides (Hem and Cropper 1959). Subsequently, these Fe (oxyhydr)oxides potentially provided additional surfaces for Fe sorption (Smith 1999). The ensuing period of a gradual increase in Fe concentration in solution and decrease in pH likely reflects the decrease in sorption sites as the surface and pores became saturated with sorbed and precipitated Fe (Figs. 10 and 12; Hashemian et al. 2013). Clinoptilolite Fe removal did not scale according to an increase in mass or surface area between small- and large-scale column experiments indicating greater solution-surface interaction with longer flow paths (Table 2).

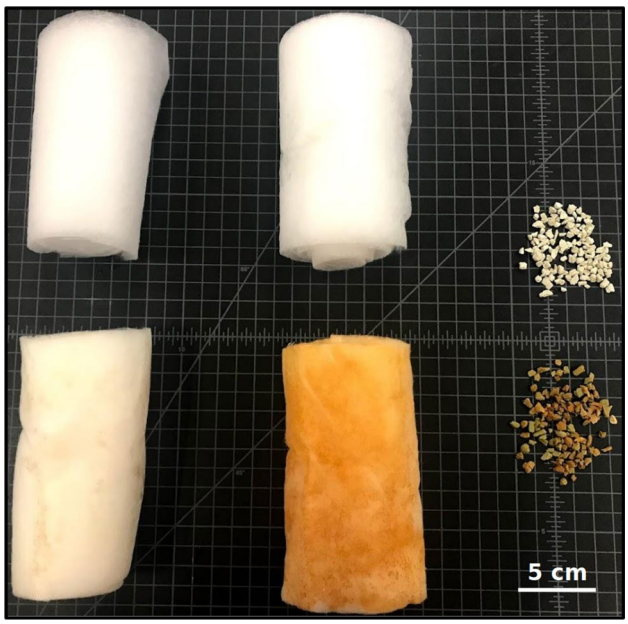

Fig. 9 Left to right: 12 g of Si, 12 g of Si + APTES, and 5.4 g of clinoptilolite before (top row) and after (bottom row) batch sorption experiments. Orange color is due to sorbed/precipitated iron (oxyhydr)oxides

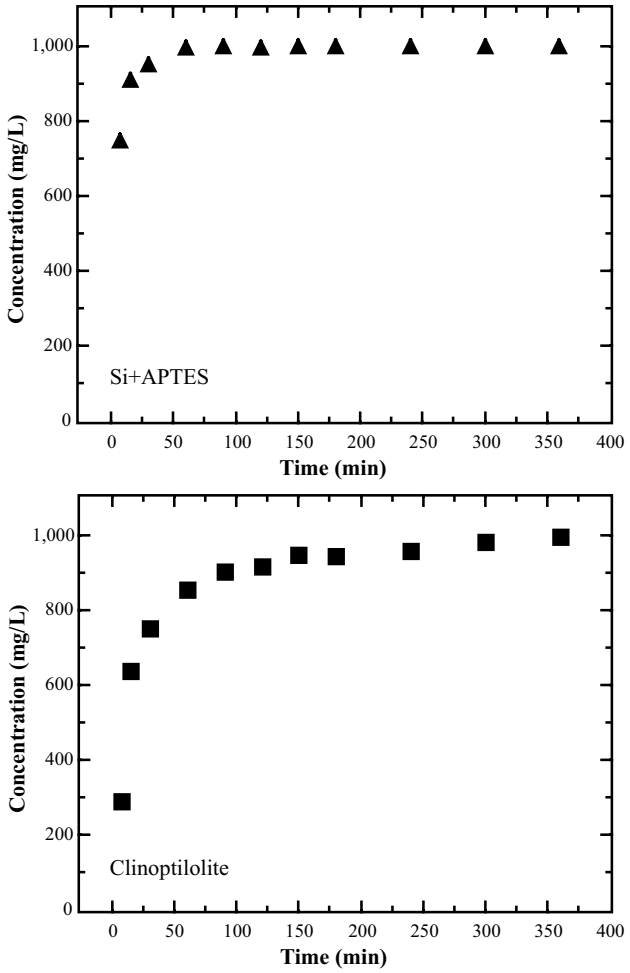

Fig. 10 Sorption of Fe^{2+} to Si + APTES (top) and clinoptilolite (bottom) in small-scale column sorption experiments

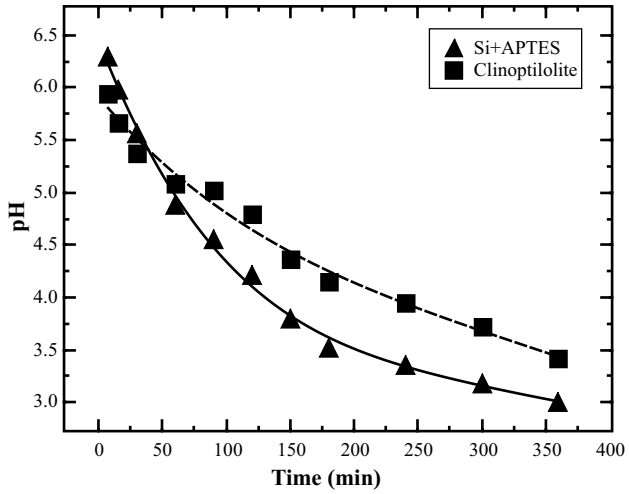

Fig. 11 pH change over the course of small-scale column sorption experiments. Initial pH of solution was 3.0 ± 0.1

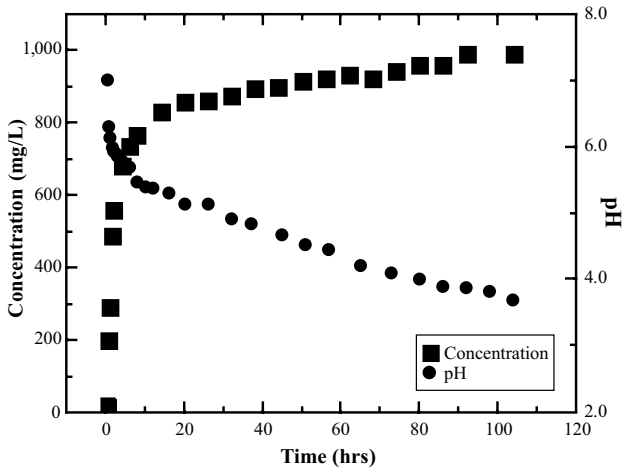

Fig. 12 Change in Fe^{2+} concentration and pH during large-scale column sorption experiments. Initial pH of solution was 3.0 ± 0.1

Table 2 Results from large- and small-scale column sorption experiments

Substrate	Mass (g)	SA[a] (m^2)	R^b_{total} (mg)	R^c_M (mg/g)	R^d_{SA} (mg/m^2)
Small-scale column					
Si + APTES	15	270	137	9.1	0.5
Clinoptilolite	150	6000	1364	9.1	0.2
Large-scale column					
Clinoptilolite	600	24,000	40,302	67.2	1.7

SA[a] square meters of surface area, R^b_{total} total milligrams of iron removed, R^c_M milligrams of iron removed per g of substrate, R^d_{SA} milligrams of iron removed per square meter of substrate surface area

Clinoptilolite Surface Alteration

The irregular surface topography and micropore structure of clinoptilolite provide a large surface area available for sorption of cations such as Fe (Pandová et al. 2018). A post-experiment evaluation of Fe distribution on the surface of clinoptilolite grains indicated diffuse capture of Fe (Fig. 13). There were concentrated areas of Fe capture, but no obvious patterns of Fe distribution across the grain surface to indicate greater capture on any topographic area or large accumulations suggestive of primary areas of mineral precipitation and growth. The entire surfaces of the clinoptilolite grains appear to have been available for metal removal by sorption and precipitation.

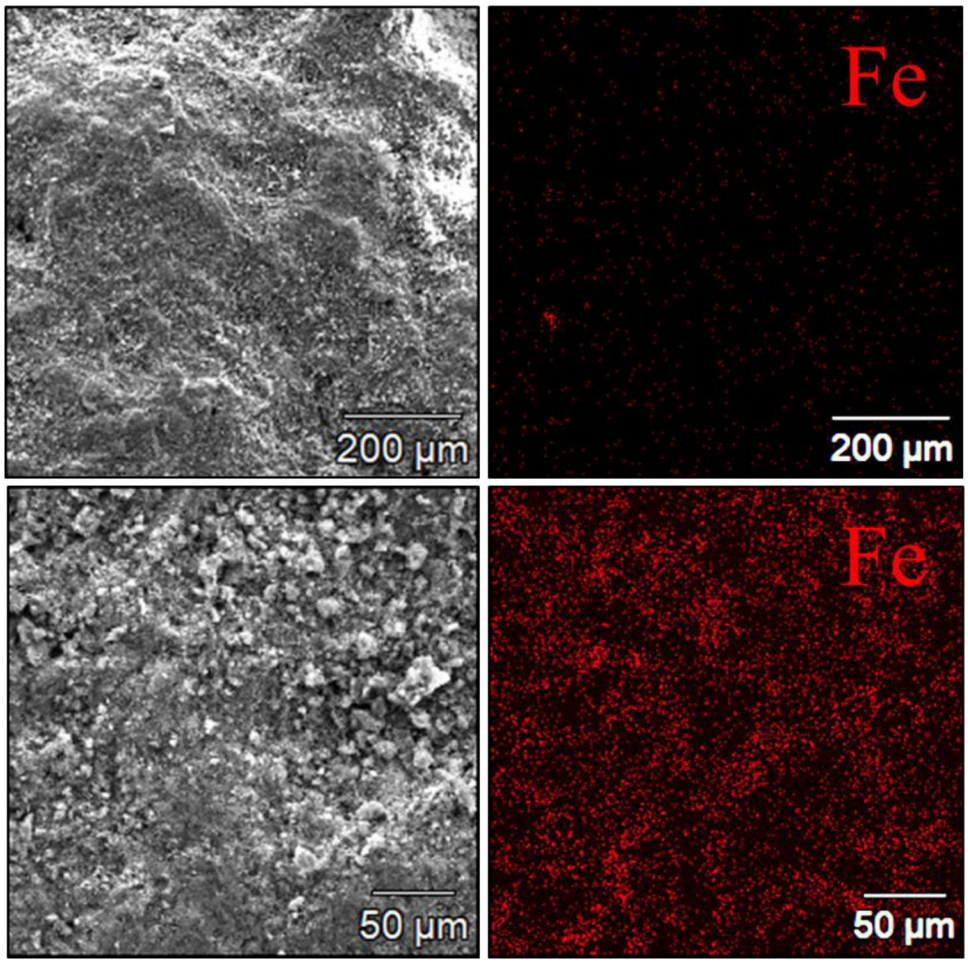

Fig. 13 (Top row) SEM image of pre-experiment clinoptilolite surface at 137 × magnification with corresponding EDS spectral map of iron. (Bottom row) SEM image of post-experiment clinoptilolite surface at 380 × magnification with corresponding EDS spectral map of iron. K_α peak was used for element identification

Conclusions

The goal of the project was to evaluate the potential use of manufactured and naturally-occurring silica/silicate forms ($pH_{pzc} \approx 3$) for passive treatment of mild (≥ pH of 3) ARD. A manufactured, noncrystalline, quartz (fused glass) fiber can be spun into a wool form that can be easily manipulated into various packing configurations and readily functionalized with a chelator such as APTES. The silicate mineral clinoptilolite (zeolite family [hydrated $(Na,K,Ca)_{2-6}Al_xSi_yO_z$]) are abundant microporous aluminosilicate grains that have the capacity to capture metals through sorption, as well as cation exchange, and are commonly referred to as "molecular sieves" because of their micropore structure. For this study, a 10-µm median diameter Si fiber (range of 5–15 µm diameter) woven into a wool was compared with a 3.6-mm median diameter clinoptilolite (range of 2.4–4.8 mm; 4 × 8 mesh) for their possible treatment system packing densities, permeability, Fe sorption efficacy under batch conditions, and ability to sorb Fe from a flowing acidic solution.

Permeability experiments indicated greater stability and permeability of the clinoptilolite under flowing conditions. Batch sorption experiments indicated an Fe specific sorption efficacy of Si + APTES > clinoptilolite > Si at equivalent surface areas. Specific sorption values normalized to possible packing densities indicated greater sorption per volume for clinoptilolite. Sorption results for Si + APTES and clinoptilolite did not produce isotherms that could be described by the Langmuir or Freundlich models, likely because of surface heterogeneity and precipitation reactions. Column sorption experiments indicated an Fe removal efficacy of clinoptilolite > Si + APTES for permeable packing densities.

Si + APTES demonstrated high specific sorption of Fe in batch sorption experiments and has potential use in low-flow, ARD passive treatment systems. The balance of greater packing stability, permeability, large surface area, micropore structure, and ion-exchange properties of clinoptilolite make these natural zeolite grains a better reactive substrate for passive treatment of mildly acidic solutions in high-flow conditions. Additionally, clinoptilolite surface preparation is minimal, and as a readily available substrate, it can easily be incorporated into construction of passive treatment systems. The clinoptilolite surface can be functionalized with a chelator such as APTES, but such an application was not

explored because of prior investigations that indicated possible clogging of the micropore structure with such a surface modification.

Acknowledgements We thank the U.S. Department of the Interior's Office of Surface Mining, Reclamation, and Enforcement; and in particular, Cecil Slaughter, for their support and funding of this project under the Applied Science Program, Cooperative Grant Agreement S17AC20000.

References

Acres RG, Ellis AV, Alvino J, Lenahan CE, Khodakov DA, Metha GF, Andersson GG (2012) Molecular structure of 3-aminopropyltriethoxysilane layers formed on silanol-terminated silicon surfaces. J Phys Chem C 116:6289–6297. https://doi.org/10.1021/jp212056s

Akcil A, Koldas S (2006) Acid mine drainage (AMD): causes, treatment and case studies. J Clean Prod 14:1139–1145. https://doi.org/10.1016/j.jclepro.2004.09.006

Aksu Z, Gönen F (2004) Biosorption of phenol by immobilized activated sludge in a continuous packed bed: prediction of breakthrough curves. Process Biochem 39:599–613. https://doi.org/10.1016/S0032-9592(03)00132-8

Baerlocher C, McCusker LB, Olson DH (2007) Atlas of zeolite framework types, 6th ed. Elsevier, Amsterdam. ISBN: 9780080554341

Barquist KN (2009) Synthesis and environmental adsorption applications of functionalized zeolites and iron oxide/zeolite composites. PhD thesis, University of Iowa. https://doi.org/10.17077/etd.xztd7s2g

Benner SG, Blowes DW, Gould WD, Herbert RB, Ptacek CJ (1999) Geochemistry of a permeable reactive barrier for metals and acid mine drainage. Environ Sci Technol 33:2793–2799. https://doi.org/10.1021/es981040u

Bigham JM, Nordstrom DK (2000) Iron and aluminum hydroxysulfates from acid sulfate waters. Rev Mineral Geochem 40:351–403. https://doi.org/10.2138/rmg.2000.40.7

Burakov AE, Galunin EV, Burakova IV, Kucherova AE, Agarwal S, Tkachev AG, Gupta VK (2018) Adsorption of heavy metals on conventional and nanostructured materials for wastewater treatment purposes: a review. Ecotoxicol Environ Saf 148:702–712. https://doi.org/10.1016/j.ecoenv.2017.11.034

Costello C (2003) Acid mine drainage: innovative treatment technologies. US EPA Office of Solid Waste and Emergency Response Technology Innovation Office, Washington, DC

Cotton A (2008) Dissolution kinetics of clinoptilolite and heulandite in alkaline conditions. Biosci Horiz 1:38–43. https://doi.org/10.1093/biohorizons/hzn003

Davis JA, Leckie JO (1978) Surface ionization and complexation at the oxide/water interface II. Surface properties of amorphous iron oxyhydroxide and adsorption of metal ions. J Colloid Interface Sci 67:90–107. https://doi.org/10.1016/0021-9797(78)90217-5

Dold B (2017) Acid rock drainage prediction: a critical review. J Geochem Explor 172:120–132. https://doi.org/10.1016/j.gexplo.2016.09.014

Dzombak DA, Morel FMM (1990) Surface complexation modeling: hydrous ferric oxide. Wiley, Oxford

Egiebor NO, Oni B (2007) Acid rock drainage formation and treatment: a review. Asia-Pac J Chem Eng 2:47–62. https://doi.org/10.1002/apj.57

Erdem E, Karapinar N, Donat R (2004) The removal of heavy metal cations by natural zeolites. J Colloid Interface Sci 280:309–314. https://doi.org/10.1016/j.jcis.2004.08.028

Faghihian H, Ghannadi Marageh M, Kazemian H (1999) The use of clinoptilolite and its sodium form for removal of radioactive cesium, and strontium from nuclear wastewater and Pb^{2+}, Ni^{2+}, Cd^{2+}, Ba^{2+} from municipal wastewater. Appl Radiat Isot 50:655–660. https://doi.org/10.1016/S0969-8043(98)00134-1

Fan C, Zhang Y (2018) Adsorption isotherms, kinetics and thermodynamics of nitrate and phosphate in binary systems on a novel adsorbent derived from corn stalks. J Geochem Explor 188:95–100. https://doi.org/10.1016/j.gexplo.2018.01.020

Felice V, Ntais S, Tavares AC (2013) Propyl sulfonic acid functionalization of faujasite-type zeolites: effect on water and methanol sorption and on proton conductivity. Micropor Mesopor Mat 169:128–136. https://doi.org/10.1016/j.micromeso.2012.10.011

Fryar AE, Schwartz FW (1998) Hydraulic-conductivity reduction, reaction-front propagation, and preferential flow within a model reactive barrier. J Contam Hydrol 32:333–351. https://doi.org/10.1016/S0169-7722(98)00057-6

Gainer GM (1993) Boron Adsorption on Hematite and Clinoptilolite. Los Alamos National Laboratory LA-SUB—93-64

Gibert O, de Pablo J, Luis Cortina J, Ayora C (2004) Chemical characterisation of natural organic substrates for biological mitigation of acid mine drainage. Water Res 38:4186–4196. https://doi.org/10.1016/j.watres.2004.06.023

Hashemian S, Hosseini SH, Salehifar H, Salari K (2013) Adsorption of Fe(III) from aqueous solution by Linde Type-A zeolite. Am J Anal Chem 4:123–126. https://doi.org/10.4236/ajac.2013.47A017

Heidmann I, Christl I, Kretzschmar R (2005) Sorption of Cu and Pb to kaolinite-fulvic acid colloids: assessment of sorbent interactions. Geochim Cosmochim Acta 69:1675–1686. https://doi.org/10.1016/j.gca.2004.10.002

Hem JD, Cropper WH (1959) Survey of ferrous-ferric chemical equilibria and redox potentials. U.S. Geological Survey Water Supply Paper 1459-A, Washington DC. https://doi.org/10.3133/wsp1459A

Holub M, Balintova M, Pavlikova P, Palascakova L (2013) Study of sorption properties of zeolite in acidic conditions in dependence on particle size. Ital Assoc Chem Eng 32:559–564. https://doi.org/10.3303/CET1332094

Johnson DB, Hallberg KB (2005) Acid mine drainage remediation options: a review. Sci Total Environ 338:3–14. https://doi.org/10.1016/j.scitotenv.2004.09.002

Kassab H, Maksoud M, Aguado S, Pera-Titus M, Albela B, Bonneviot L (2012) Polyethylenimine covalently grafted on mesostructured porous silica for CO_2 capture. RSC Adv 2:2508–2516. https://doi.org/10.1039/C2RA01007K

Kefeni KK, Msagati TAM, Mamba BB (2017) Acid mine drainage: prevention, treatment options, and resource recovery: a review. J Clean Prod 151:475–493. https://doi.org/10.1016/j.jclepro.2017.03.082

Langmuir I (1918) The Adsorption of gases on plane surfaces of glass, mica and platinum. J Am Chem Soc 40:1361–1403. https://doi.org/10.1021/ja02242a004

Limousin G, Gaudet JP, Charlet L, Szenknect S, Barthès V, Krimissa M (2007) Sorption isotherms: a review on physical bases, modeling and measurement. Appl Geochem 22:249–275. https://doi.org/10.1016/j.apgeochem.2006.09.010

Liu Y, Li Y, Li XM, He T (2013) Kinetics of (3-aminopropyl) triethoxylsilane (APTES) silanization of superparamagnetic iron oxide nanoparticles. Langmuir 29:15275–15282. https://doi.org/10.1021/la403269u

Motsi T, Rowson NA, Simmons MJH (2009) Adsorption of heavy metals from acid mine drainage by natural zeolite. Int J Miner Process 92:42–48. https://doi.org/10.1016/j.minpro.2009.02.005

Nelson J, Joe-Wong CM, Maher K (2019) Cr(VI) reduction by Fe(II) sorbed to silica surfaces. Chemosphere 234:98–107. https://doi.org/10.1016/j.chemosphere.2019.06.039

Nordstrom DK (2009) Acid rock drainage and climate change. J Geochem Explor 100:97–104. https://doi.org/10.1016/j.gexplo.2008.08.002

Nordstrom DK (2011) Mine waters: acidic to circumneutral. Elements 7:393–398. https://doi.org/10.2113/gselements.7.6.393

Nordstrom DK, Alpers CN (1999) Negative pH, efflorescent mineralogy, and consequences for environmental restoration at the Iron Mountain Superfund site, California. Proc Natl Acad Sci 96:3455–3462. https://doi.org/10.1073/pnas.96.7.3455

Nordstrom DK, Blowes DW, Ptacek CJ (2015) Hydrogeochemistry and microbiology of mine drainage: an update. Appl Geochem 57:3–16. https://doi.org/10.1016/j.apgeochem.2015.02.008

Pandová I, Panda A, Valíček J, Harničárová M, Kušnerová M, Palková Z (2018) Use of sorption of copper cations by clinoptilolite for wastewater treatment. Int J Environ Res Public Health 15:1364. https://doi.org/10.3390/ijerph15071364

Ramasamy DL, Khan S, Repo E, Sillanpää M (2017) Synthesis of mesoporous and microporous amine and non-amine functionalized silica gels for the application of rare earth elements (REE) recovery from the waste water-understanding the role of pH, temperature, calcination and mechanism in light REE and heavy REE separation. Chem Eng J 322:56–65. https://doi.org/10.1016/j.cej.2017.03.152

Ramasamy DL, Puhakka V, Iftekhar S, Wojtuś A, Repo E (2018) N- and O-ligand doped mesoporous silica-chitosan hybrid beads for the efficient, sustainable and selective recovery of rare earth elements (REE) from acid mine drainage (AMD): understanding the significance of physical modification and conditioning of the polymer. J Hazard Mater 348:84–91. https://doi.org/10.1016/j.jhazmat.2018.01.030

Sandlin W, Langman J, Moberly J (2020) A review of acid rock drainage, seasonal flux of discharge and metal concentrations, and passive treatment system limitations. Int J Min Reclam Environ. https://doi.org/10.1080/17480930.2020.1728035

Skousen J, Zipper CE, Rose A, Ziemkiewicz PF, Nairn R, McDonald LM, Kleinmann RL (2017) Review of passive systems for acid mine drainage treatment. Mine Water Environ 36:133–153. https://doi.org/10.1007/s10230-016-0417-1

Smith KS (1999) Metal sorption on mineral surfaces: an overview with examples relating to mineral deposits. In: Proc, Environmental Geochemistry Of Mineral Deposits, Part A. processes, techniques, and health issues, pp 161–182. https://doi.org/10.5382/Rev.06.07

Stumm W, Morgan JJ (1996) Aquatic chemistry: chemical equilibria and rates in natural waters, 3rd edn. Wiley, Oxford

Stylianou MA, Hadjiconstantinou MP, Inglezakis VJ, Moustakas KG, Lizidou MD (2007) Use of natural clinoptilolite for the removal of lead, copper and zinc in fixed bed column. J Hazard Mater 143:575–581. https://doi.org/10.1016/j.jhazmat.2006.09.096

Vilarrasa-García E, Cecilia JA, Moya EMO, Cavalcante CL, Azevedo DCS, Rodríguez-Castellón E (2015) "Low cost" pore expanded SBA-15 functionalized with amine groups applied to CO_2 adsorption. Materials 8:2495–2513. https://doi.org/10.3390/ma8052495

Wang S, Peng Y (2010) Natural zeolites as effective adsorbents in water and wastewater treatment. Chem Eng J 156:11–24. https://doi.org/10.1016/j.cej.2009.10.029

Wingenfelder U, Nowack B, Furrer G, Schulin R (2005) Adsorption of Pb and Cd by amine-modified zeolite. Water Res 39:3287–3297. https://doi.org/10.1016/j.watres.2005.05.017

Yavuz Ö, Altunkaynak Y, Güzel F (2003) Removal of copper, nickel, cobalt and manganese from aqueous solution by kaolinite. Water Res 37:948–952. https://doi.org/10.1016/S0043-1354(02)00409-8

Zhu M, Lerum MZ, Chen W (2012) How to prepare reproducible, homogeneous, and hydrolytically stable aminosilane-derived layers on silica. Langmuir 28:416–423. https://doi.org/10.1021/la203638g